Received: 17 October 2023 | Revised: 13 December 2023 | Accepted: 4 January 2024

DOI: 10.1002/inf2.12534

RESEARCH ARTICLE

WILEY

An intelligent self-powered life jacket system integrating multiple triboelectric fiber sensors for drowning rescue

Yiping Zhang[1,2] | **Chengyu Li**[1,3] | **Chuanhui Wei**[1,3] | **Renwei Cheng**[1,3] | **Tianmei Lv**[1,3] | **Junpeng Wang**[2] | **Cong Zhao**[2] | **Zhaoyang Wang**[2] | **Fangming Li**[2] | **Xiao Peng**[1,3] | **Minyi Xu**[2] | **Kai Dong**[1,3]

[1]CAS Center for Excellence in Nanoscience, Beijing Key Laboratory of Micro-Nano Energy and Sensor, Beijing Institute of Nanoenergy and Nanosystems, Chinese Academy of Science, Beijing, the People's Republic of China

[2]Dalian Key Lab of Marine Micro/Nano Energy and Self-Powered Systems, Marine Engineering College, Dalian Maritime University, Dalian, the People's Republic of China

[3]School of Nanoscience and Technology, University of Chinese Academy of Sciences, Beijing, the People's Republic of China

Correspondence

Minyi Xu, Dalian Key Lab of Marine Micro/Nano Energy and Self-Powered Systems, Marine Engineering College, Dalian Maritime University, Dalian, 116026, the People's Republic of China.
Email: xuminyi@dlmu.edu.cn

Kai Dong, CAS Center for Excellence in Nanoscience, Beijing Key Laboratory of Micro-Nano Energy and Sensor, Beijing Institute of Nanoenergy and Nanosystems, Chinese Academy of Science, Beijing 101400, the People's Republic of China.
Email: dongkai@binn.cas.cn

Funding information

Natural Science Foundation of the Beijing Municipality, Grant/Award Numbers: L222037, 2212052; National Natural Science Foundation of China, Grant/Award Number: 22109012; Fundamental Research Funds for the Central Universities, Grant/Award Number: E1E46805

Abstract

The inherent unpredictability of the maritime environment leads to low rates of survival during accidents. Life jackets serve as a crucial safety measure in underwater environments. Nonetheless, most conventional life jackets lack the capability to monitor the wearer's underwater body movements, impeding their effectiveness in rescue operations. Here, we present an intelligent self-powered life jacket system (SPLJ) composed of a wireless body area sensing network, a set of deep learning analytics, and a human condition detection platform. Six coaxial core-shell structure triboelectric fiber sensors with high sensitivity, stretchability, and flexibility are integrated into this system. Additionally, a portable integrated circuit module is incorporated into the SPLJ to facilitate real-time monitoring of the wearer's movement. Moreover, by leveraging the deep-learning-assisted data analytics and establishing a robust correlation between the wearer's movements and condition, we have developed a comprehensive system for monitoring drowning individuals, achieving an outstanding recognition accuracy of 100%. This groundbreaking work introduces a fresh approach to underwater intelligent survival devices, offering promising prospects for advancing underwater smart wearable devices in rescue operations and the development of ocean industry.

KEYWORDS

deep learning, intelligent life jackets, movement recognition, self-powered, triboelectric fiber sensors

Yiping Zhang, Chengyu Li, and Chuanhui Wei contributed equally to this work.

1 | INTRODUCTION

The maritime industry has experienced substantial growth driven by societal and economic advancements, leading to increased participation in marine construction and maritime transportation. However, the inherent unpredictability of the maritime environment gives rise to significant accident risks. The survival rate of individuals who fall into the water is severely compromised by inhospitable marine conditions, such as extremely low water temperatures and limited availability of maritime assistance.[1–3] According to statistics from the International Maritime Organization, prolonged exposure to cold seawater will cause heat loss, resulting in hypothermia and accounting for 80% of fatalities in maritime accidents.[4] Additionally, rescue teams frequently encounter difficulties in obtaining timely and crucial information about distressed individuals, hindering the development of effective rescue strategies, and contributing to preventable loss of life.

Life jackets have long been considered the ultimate line of protection for individuals at sea. Traditional life jackets primarily provide buoyancy and thermal insulation. For example, Liu et al. designed a self-heating life jacket that incorporates an internal self-heater for heat dissipation.[5] Han et al. developed a self-heating inflatable life jacket that utilizes the chemical energy of a gas generator to facilitate rapid inflation.[6] However, the absence of monitoring capabilities in these life jackets complicates the formulation of real-time rescue strategies. In response, some researchers attempt to monitor individuals' physiological activity underwater, For instance, Zou et al. proposed a bio-inspired stretchable nanogenerator, drawing inspiration from electric eels, for underwater energy harvesting and posture sensing.[7] Nevertheless, these discrete sensors require attachment to multiple body parts, rendering them susceptible to interference from body movements and crosstalk.[8–10] In addition, there are also significant deficiencies in wearing comfort and maneuverability.[11,12] Wireless body area network (WBAN) is a wireless network technology that connects tiny nodes with sensors in or around a person. This technology enables a more effective distribution of sensors, thereby enhancing user comfort and facilitating greater flexibility of movement while providing the best possible monitoring.[13–15] For example, Rasyide utilized WBAN technology to design a mountaineer monitoring life jacket, enabling real-time monitoring of the mountaineer's physiological state and information sharing.[16] However, this work is not water-resistant to the devices and shows inadequate for underwater environments.[17–20] Therefore, there is an urgent need for a comfortable and intelligent life jacket, adept at real-time monitoring of the wearer's movement status in aquatic environments.

Wearable textile sensors based on the triboelectric effect[21,22] have recently gained prominence in human activity monitoring due to their excellent performance in detecting low-frequency and small-scale motions.[23–26] By combining with this exciting development, life jackets are expected to be used for underwater movement monitoring.[27–31] Here, a comfortable and intelligent self-powered life jacket (SPLJ) for monitoring the movements of individuals at risks is reported, which is designed based on the WBAN and deep learning analytics. In detail, six triboelectric fiber sensors with high sensitivity, stretchability, and flexibility are affixed to the shoulders, knees and elbows to build WBAN, which allows the extraction of movement characteristics of the human movement states more accurately. Upon an individual falls into the water, the triboelectric fiber sensors integrated into the SPLJ promptly capture real-time movement states by effectively converting motion signals into electrical counterparts. These electrical signals are processed instantaneously using a portable integrated circuit module and transmitted wirelessly to the rescue terminal. At the rescue terminal, real-time processing and data analysis are carried out via the convolutional neural networks (CNNs) analytics, enabling the extraction of crucial information about the individual's movements. Leveraging the well-established correlation between movements and hypothermic condition, we achieve precise assessments of individual's physiological state. Consequently, the rescue team can develop tailored rescue strategies to optimize the individual's chances of survival. The developed SPLJ introduces a novel and effective approach to underwater human activity monitoring, while the real-time information transmission and feedback capabilities facilitated by WBAN significantly enhance the efficiency and accuracy of rescue operations, thus ushering in new possibilities in the realm of maritime survival.

2 | RESULTS AND DISCUSSION

2.1 | Design and composition of SPLJ system

Figure 1A depicts a closed-loop feedback system for drowning movements monitoring and distress rescue based on SPLJ, which is centered on the People's Republic of China technology. In the event of a person falling into the water, the SPLJ system transforms human body movements into electrical signals. These signals are then transmitted wirelessly to a designated rescue

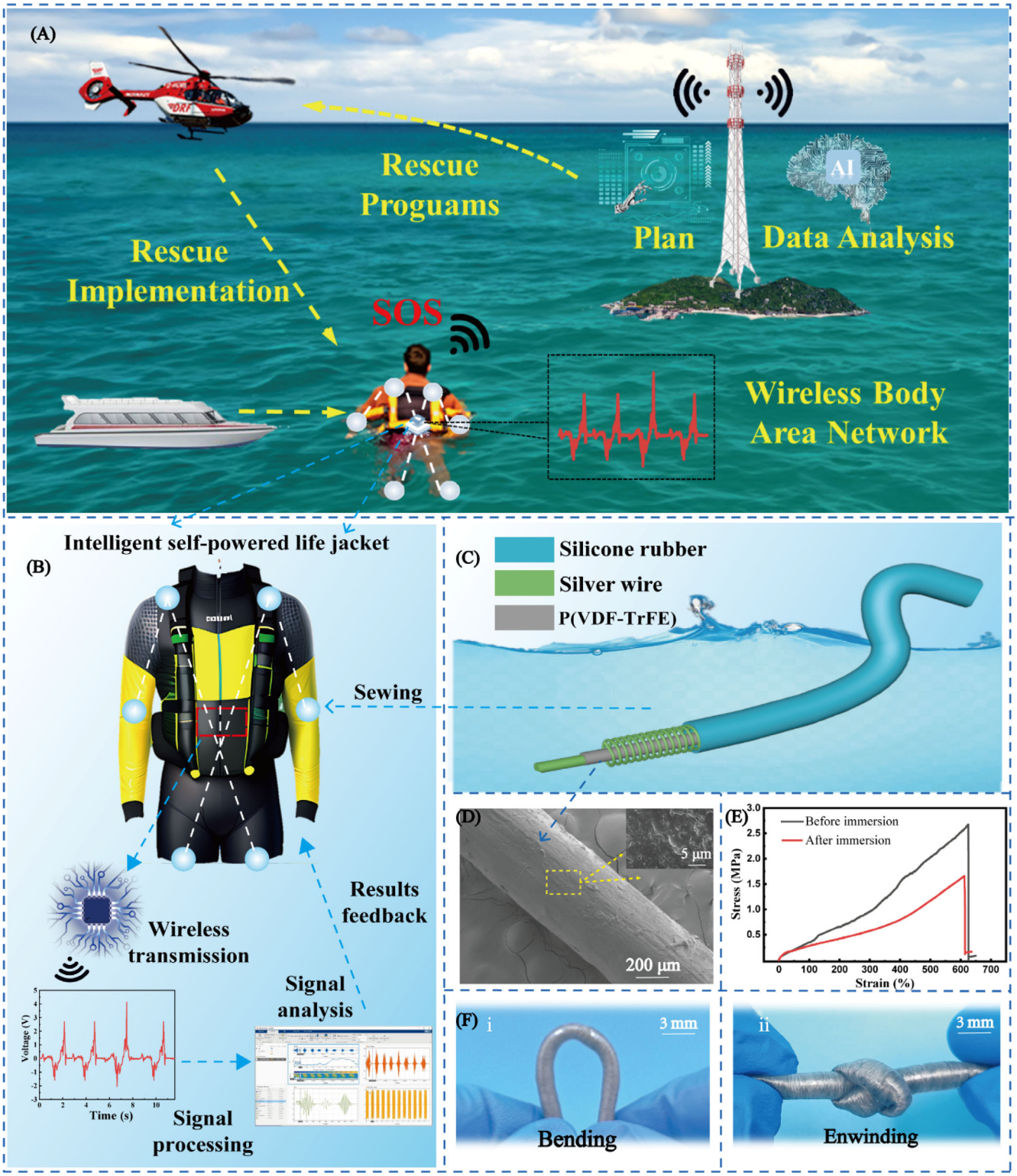

FIGURE 1 Design and structure of the SPLJ. (A) Schematic diagram of the real-time monitoring process of the SPLJ. (B) The framework of SPLJ system. (C) The structure of triboelectric fiber sensor. (D) The SEM image of the P(VDF-TrFE) fiber. (E) Uniaxial tensile test of triboelectric fiber sensor before and after 72-h immersion in seawater. (F) Photographs of the triboelectric fiber sensor under (i) bending and (ii) enwinding state.

center. At the rescue center, data analysis is conducted to assess the condition of the drowning individual and to formulate a corresponding rescue strategy. Figure S1 illustrates the workflow of the SPLJ system. The schematic representation of the SPLJ structure is presented in Figure 1B. SPLJ incorporates components such as the

WBAN, portable integrated circuit module (signal acquisition, processing, filtering, and transmission) data analysis, and condition monitoring interface. As the fundamental sensing component of the WBAN, six triboelectric fiber sensors, are strategically sewn at the shoulders, elbows, and knees (as shown in Figure S2). The specific structure of the triboelectric fiber sensor is displayed in Figure 1C. Maritime environments are characterized by complex geography and ecosystems, while a large amount of water will carry away the charges generated on contact surface.[32–35] Therefore, it is necessary to select a self-powered sensor with a vertical contact separation mode that is simple and durable to enhance the sensitivity and robustness of the sensor. The coaxial core-shell structure is employed to create an ideal contact-separation space,[36] while its contact sensing direction has been expanded to a full 360°. Moreover, this structure is easy to fabricate and suitable for large-scale industrial production, making it an excellent choice for underwater sensing applications (as depicted in Figure S3).

Because of its good electrical conductivity and elasticity, the silver wire is chosen as the electrode as well as the triboelectric material for the shell structure. The organic piezoelectric material poly (vinylidene fluoride-trifluoroethylene) (P(VDF-TrFE)) is utilized as another triboelectric material. As depicted in Figure 1D, scanning electron microscopy (SEM) reveals that the P(VDF-TrFE) fiber exhibits a relatively smooth surface with microstructure at the nanoscale, which is suitable for triboelectric materials. To maintain the integrity of the internal structure and prevent contamination, silicone rubber is employed for water sealing, enhancing hydrophobicity and corrosion resistance. The fabrication process of triboelectric fiber sensor is illustrated in Figure S4. The core and shell are prepared respectively (see the Section 4 for specific preparation methods) and then assembled by silicone rubber to fabricate triboelectric fiber sensor. As an underwater monitoring device, it is crucial to possess waterproof and corrosion-resistant properties. Hence, we conducted mechanical tests on the device before and after immersing it in seawater for 72 h. The results shown in Figure 1E indicate that the device displayed minimal changes when stretched to less than 50%. It is worth noting that the tensile elongation required for human body movement falls within this range, indicating the device's superior chemical stability. While wearing the sensor in an underwater environment, it is necessary to ensure that the device does not impede movement. As displayed in Figure 1F, the sensor should be designed with unique material selection and structural design for excellent flexibility.

2.2 | Performance characterization of triboelectric fiber sensor

Good sensing performance is essential for practical applications. To simulate real-life scenarios, we construct an underwater monitoring system by combining a linear motor with acrylic plates. The system continuously impacts the triboelectric fiber sensor to simulate external excitation, as illustrated in Figure S5. The working principle of the triboelectric fiber sensor is demonstrated in Figure 2A. Using the arm movement as an example, in the initial state, there is no contact between the silver wire and P(VDF-TrFE), resulting in charge-balance and no electron flow in the external circuit. When the arm is bent, the distance between two triboelectric layers gradually decreases. This leads to charge transfer and electron flow in the external circuit. Conversely, when the arm is straightened, the distance between the two triboelectric layers gradually increases, driving the flow of free electrons in the opposite direction, resulting in a reverse electrical. Under the continuous application of the arm's movement, the triboelectric layers continuously contact and separate. It generates an alternating electrical signal in the external circuit. Figure 2B displays the simulation of the electrical potential changes at each part in the process of contact and separation. The P(VDF-TrFE) is annealed to improve the output performance of triboelectric fiber sensor underwater, as the principle is depicted in Figure S6. It can be observed that the ferroelectric phase β in P(VDF-TrFE) is formed due to annealing. The interaction between positive and negative charges generates a microscopic electric field during contact electrification. Furthermore, the originally disordered electric dipoles in the ferroelectric phase align in an organized manner along the direction of the electric field lines. This alignment is known as ferroelectric polarization. Ferroelectric polarization creates a new microelectric field within P(VDF-TrFE), enhancing its electron acquisition capability and then improving output performance.[37,38]

Under the continuous impact of the linear motor, the triboelectric fiber sensor generates continuous AC electrical signal. The temperature and air pressure are kept at 298 K and 101 kPa, respectively. The linear motor's maximum distance per cycle is set at 20 cm. In movement monitoring, force and frequency are two important characterizing parameters, so it is necessary to test the triboelectric fiber sensors' response to different forces and different frequencies. Maintaining a frequency of 1 Hz, forces ranging from 1 to 5 N are applied to lightly impact the triboelectric fiber sensor. And its response to the applied force is measured. The results, as shown in Figure 2C, indicate that under a force of 1 N, the open-

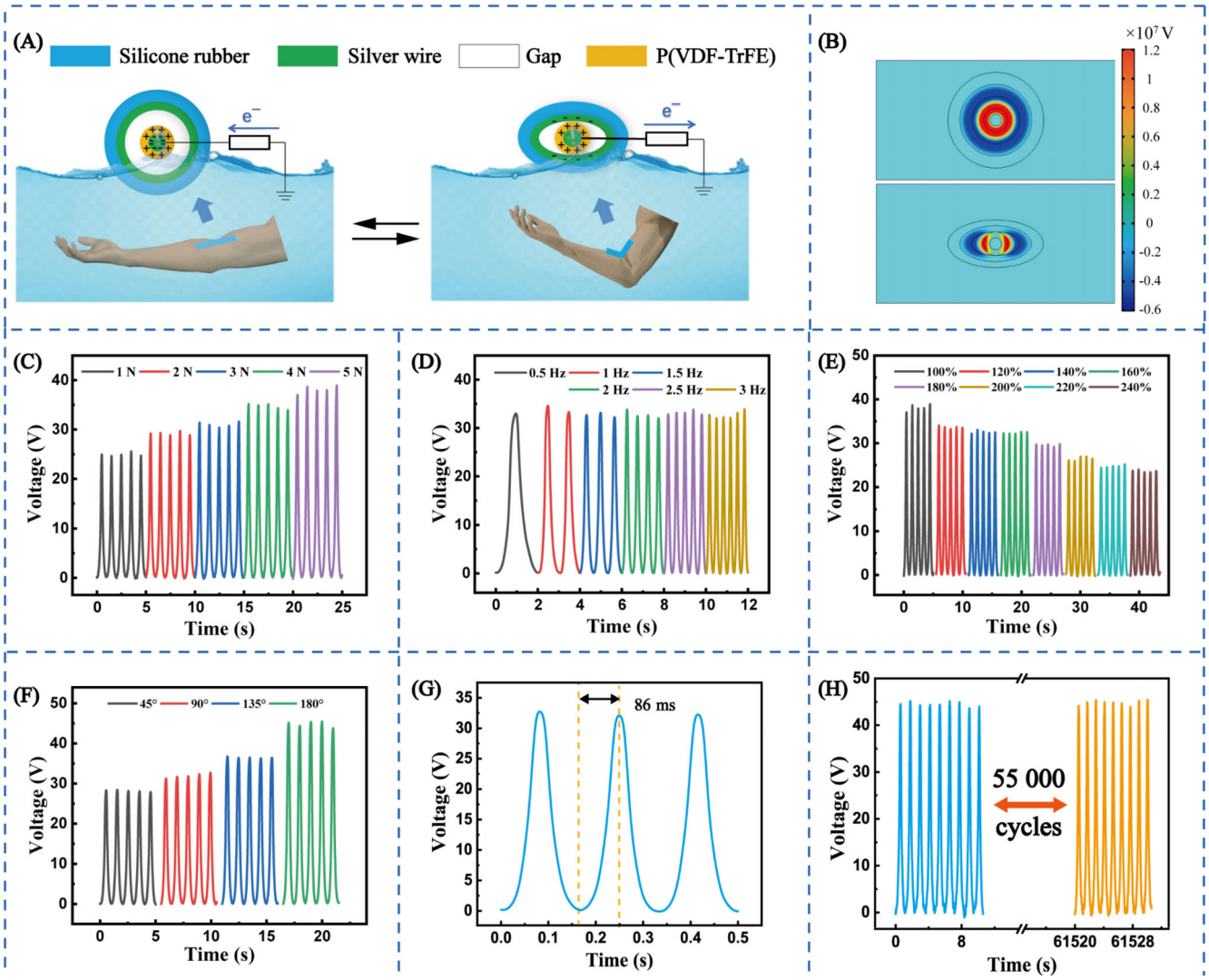

FIGURE 2 Working principle and output performance characterization of triboelectric fiber sensor. (A) Charge distribution diagram of triboelectric fiber sensor in arm movement, under the condition of external resistance. (B) Numerical calculations of the potential distribution of triboelectric fiber sensor under open-circuit conditions using the COMSOL software. Electrical output voltage of triboelectric fiber sensor (length 5 cm) with a constant applied load at different (C) forces, (D) frequencies, (E) strains during impacting, (F) and bending angles during impacting. (G) Response time of triboelectric fiber sensor. (H) 55 000 times fatigue testing of triboelectric fiber sensor.

circuit voltage is 24.7 V, while the short-circuit current and transferred charge are 64.1 nA and 8.7 nC, respectively (as shown in Figure S7). As the force gradually increases, the output of the triboelectric fiber sensor also increases. When the force reaches 5 N, the open-circuit voltage rises to 33.5 V, while the short-circuit current and the transferred charge are 107.3 nA and 11.8 nC, respectively. The response of the triboelectric fiber sensor to frequency under a force of 2 N is discussed next (Figure 2D). The results show that as the frequency increases from 0.5 to 3 Hz, the output voltage remains relatively constant at around 34 V. The output charge also stabilizes at around 11.6 nC. And the short-circuit current increases from 52.8 nA at 0.5 Hz to 198.9 nA (as shown in Figure S8). It can be seen that the signal effectively characterizes the frequency changes in external excitation, fulfilling the necessary requirements for underwater sensor characteristics. Furthermore, since the triboelectric fiber sensors are worn on the joints, they are expected to have excellent output performance under stretching and bending states. The output performance of the triboelectric fiber sensor, when subjected to different strains during impact, is also examined (Figure 2E). As the strain increases, the triboelectric fiber sensor output gradually decreases from 100% of nearly 40 V to 240% of 24 V. The decrease in output voltage can be attributed to the deformation of the silicone rubber as the strain increases. This deformation reduces the gap between the

silver wire and P(VDF-TrFE), resulting in a decrease in the output voltage. Similarly, the short-circuit current and transferred charge decrease from 107.3 nA and 16.5 nC to 85.5 nA and 9 nC, respectively (Figure S9). The relationship between the triboelectric fiber sensor output and the bending angle under the same force impacting is also investigated, as shown in Figure 2F. It can be observed that the voltage output gradually increases as the bending angle increased while maintaining the impacting, showcasing its ability to maintain outstanding characteristics even under bending conditions. This is because a greater bending angle enhances the contact between P(VDF-TrFE) and the silver wire, and the triboelectric fiber sensor output is positively correlated with the extent of contact between the materials. Similarly, the short-circuit current increases from 71.8 to 125.3 nA, and the transferred charge increases from 9.8 to 15.1 nC, respectively (Figure S10). From the previous section, it is apparent that these triboelectric fiber sensors are versatile in adapting to various body movements. The triboelectric fiber sensor exhibits a fast response time of 86 ms. This allows an accurate electrical signal to be generated even with very brief contact (Figure 2G). To assess the durability of the triboelectric fiber sensor, it is repetitively used 55 000 times under normal conditions. Its output performance remains unchanged and demonstrates high durability with no significant degradation or variation (Figure 2H). Additionally, the stability after multiple operations in water is also considered. Even after stirring for 18 times, the electrical output shows no significant drop (Figure S11). Since the life-saving equipment may be placed for a long time without real-time inspection. The triboelectric fiber sensor is storied in a typical environment for 1 month, the performance of the triboelectric fiber sensor shows no obvious degradation (Figure S12). Furthermore, the temperature of seawater varies from different maritime regions, so it is crucial to investigate how fluctuations in temperature in the environment affect output performance. The triboelectric fiber sensor is underwent multiple washes in water for 10 min and dried in the drying oven, then test the output performance with a continued impact. The results are shown in Figure S13, the detection signal is almost stable (ranging from 10 to 20°C) with only 2.74% output attenuation.

2.3 | Correlation between movements and condition of a drowning person

Due to its remarkable flexibility, stretchability, and mechanical responsiveness, the triboelectric fiber sensor is highly suitable for wearable monitoring of human body movements. By utilizing WBAN technology, the triboelectric fiber sensors are integrated onto the SPLJ which is positioned on the elbows and knees, as depicted in Figure 3A,B. The findings reveal that the output voltage exhibits a corresponding response at varying bending angles. after the triboelectric fiber sensors are sewn onto the apparel. If the individual is immersed in water for a long period of time, the body may tremble. Tremors are currently classified into five levels based on their vibration amplitudes: Level 0 indicates no tremor, Level 1 indicates mild tremor, Level 2 indicates tremor with an amplitude of 0.5–1 cm, Level 3 indicates tremor with an amplitude of 1–2 cm, and Level 4 indicates tremor exceeding 2 cm.[39] Therefore, we monitor the output response of the triboelectric fiber sensor at the arm joints under different tremor levels (as shown in Figure 3C). It can be observed that as the amplitude of the tremor increases, the response output of triboelectric fiber sensor also increases. Based on the excellent triboelectric fiber sensor performance and WBAN technology, the SPLJ system has been developed. The portable integrated circuit module for the SPLJ system is depicted in Figure 3D. The circuit module consists of an STM32-controlled Wi-Fi module, an AD acquisition module, and a charge amplifier. It is responsible for stabilizing, filtering, and wirelessly transmitting the signals collected by the triboelectric fiber sensor to a computer terminal. Due to its exceptional chemical stability, high flexibility, and integration, the SPLJ system is utilized to monitor the movements and condition of the drowning individuals. The actual image, shown in Figure 3E, displays that the WBAN comprises six components, and the circuitry is securely integrated inside the life jacket, ensuring the reliability and safety of the system for consistent operation. Additionally, in order to ensure that SPLJ won't compromise the movement flexibility of the drowning individual, various movements, such as bending and stretching, are performed when wearing SPLJ, as depicted in Figure S14. This demonstration confirms that SPLJ does not hinder the users' movements.

The survival of an individual in underwater conditions is influenced by various factors such as water temperature, salinity, duration of submersion, and the age of the victim. Therefore, we focus on the marine environment in the central part of the Yellow Sea in China, which exhibits water temperatures ranging from 4 to 10°C and salinity level of 32–34‰. In this experiment, we consider the scenario of a 24-year-old adult male falling into the water and examine the changes in his physical condition during submersion. As shown in Figure 3F, to simulate the actual rescue environment, we divide the submersion period into the following five stages: After falling into the water, the drowning person starts

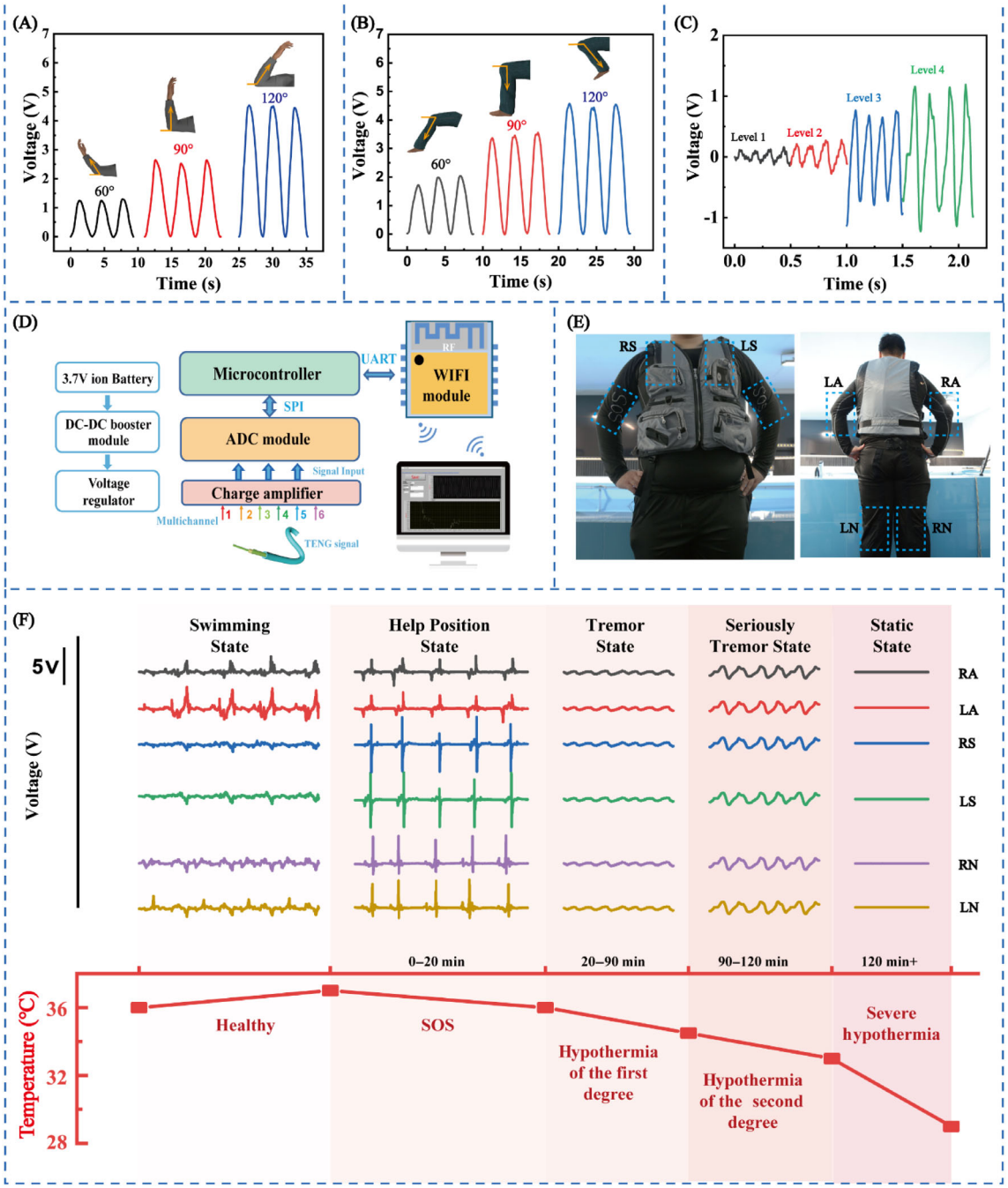

FIGURE 3 Signal outputs of SPLJ and the correlation between movements and drowning human condition. The voltage output signal of different (A) elbow, (B) knees bending angle by programmable electrostatic voltmeter. (C) The output response of triboelectric fiber sensor at the arm joints under different tremor levels. (D) Schematic diagram of the portable integrated circuit module. (E) Photographs of SPLJ worn on the drowning person. (F) The signal outputs of SPLJ in different movements of drowning person and the correlation between the signal and human condition.

swimming to find a safe location and await rescue. During this phase, the body temperature may slightly increase due to physical activity, representing the healthy phase. Once a safe position is reached, the drowning person ceases swimming to conserve energy and assumes the HELP position to minimize heat loss. In this stage, referred to as the SOS phase, is characterized by seeking external assistance and a gradual decrease in body temperature. This stage lasts for approximately 20 min. Subsequently, the person enters the hypothermia stage. Hypothermia can be classified into four stages based on its progression: Stage 1 hypothermia, characterized by tremor, increased heart rate, and muscle coordination impairment; Stage 2 hypothermia is characterized by

severe tremor, weakness, and cognitive numbness; Stage 3 hypothermia, marked by the absence of tremor and reflexes; and Stage 4 hypothermia is marked by muscle rigidity and difficulty detecting heartbeat and respiration. During the 20–90 min period after submersion, the person experiences mild tremor, and the body temperature gradually decreases to 34°C, indicating Stage 1 hypothermia. Between 90 and 120 min, the intensity of tremors increases, and the body temperature further drops to 33°C, indicating Stage 2 hypothermia. If submersion exceeds 120 min, tremor ceases, and body temperature declines to 28°C, indicating severe hypothermia. In addition to monitoring the physical condition of a drowning person, this system can also be applied to posture monitoring in daily life (Figure S15), such as monitoring standing, walking, running, and squatting positions. There is a noticeable alteration in the voltage peaks compared to the prior test. Two factors contribute to this phenomenon: (1) electrostatic shielding when the SPLJ is submerged in water reduce the output. (2) The circuit module which generates an analog signal in the form of a current–voltage signal is utilized to transmit the signal, cause an output decrease. Since subsequent experiments are utilizing the circuit module, the disparity do not affect the signal processing and deep learning.

2.4 | Analysis of signals in detail for different movements

To further validate the effectiveness of SPLJ, the commercial monitoring sensors are employed to conduct comparative tests with subjects performing identical actions. This facilitates an examination of the correlation between the signals from SPLJ and human body movements. The commercial monitoring sensors are placed at the subject's forearm joints to analyze the human movement process along with the two types of signals. The results, as shown in Figure 4A, demonstrate a strong correlation between the pitch angle output of the commercial monitoring sensors and the voltage curve of SPLJ. This finding conclusively proves the exceptional motion monitoring capability of the SPLJ. Moreover, compared to the commercial monitoring sensors, the SPLJ exhibits a faster response time and the ability to detect motion frequency and oscillation, thereby enabling a more comprehensive capture of motion-related information. Additionally, a linear relationship between the bending angle of the arm and the output signal of SPLJ is observed, as shown in Figure 4B.

To further analyze the signals of each movement, we extract the average peak values of the movement signals and employ the information obtained from the SPLJ to identify the specific state of the drowning individual (Figure S16). The findings reveal distinct characteristics in the movement signal amplitudes during various movements. During swimming, the highest movement signal amplitude is observed in the arms, followed by the legs, while the shoulder exhibits a relatively smaller amplitude. This difference can be attributed to the larger range of motion in the arms and legs compared to the shoulder. In the HELP position, the movement signal amplitude is highest in the shoulders, followed by the arms and legs. This is because the drowning person is tapping the shoulders, generating a larger signal in that region. During the tremor period, the movement signal amplitudes of the shoulders, arms, and legs are all relatively small. This is because tremor motions have smaller amplitudes, resulting in smaller generated signals. When the drowning person is static, the movement signal amplitudes approach zero, indicating a significant loss of mobility. Therefore, SPLJ no longer generates noticeable movement signals (Figure 4C). To provide a detailed analysis of the movement signals during normal swimming, the HELP position, and tremor, we incorporate inertial measurement modules to monitor the movement processes of the drowning individual (Figure 4D).

The results for the HELP position test are presented in Figure 4E. During the assessment, the subjects perform various actions, including arm bending, crossing arms in front of the chest, arm resetting, bringing legs to the abdomen, and leg extension resetting. Notably, both the pitch output angle of the commercial monitoring sensors placed on the arms, shoulders, and legs, as well as the voltage curve of the SPLJ, exhibit a strong correlation. It should be noticed that the legs remain partially bended due to the buoyancy, which causes the pitch angle of the gyroscope did not return to zero. The test outcomes for swimming are illustrated in Figure S17. Subjects execute movement such as the initial stroke position, hand stroke and leg bend, hand hug and foot flip, and arm extension kick. In these cases, the roll output angle of the commercial monitoring sensors on the arms and legs shows a significant correlation with the voltage curve of the SPLJ. Frequency domain analysis is employed better to represent the swimming stroke process of the arms. Figure S18 demonstrates the tremor signal. As the degree of trembling increased, both the accelerometer values and the motion signal of the intelligent lifejacket gradually intensified. To account for individual differences, subjects with varying heights and weights are selected to evaluate the universality of the SPLJ signal. The results, shown in Figure 4F–H, reveal consistent trends in the motion representation signal of the SPLJ across different subjects. This outcome substantiates the SPLJ's universality in movement monitoring and underscores its significant potential in the field of underwater rescue.

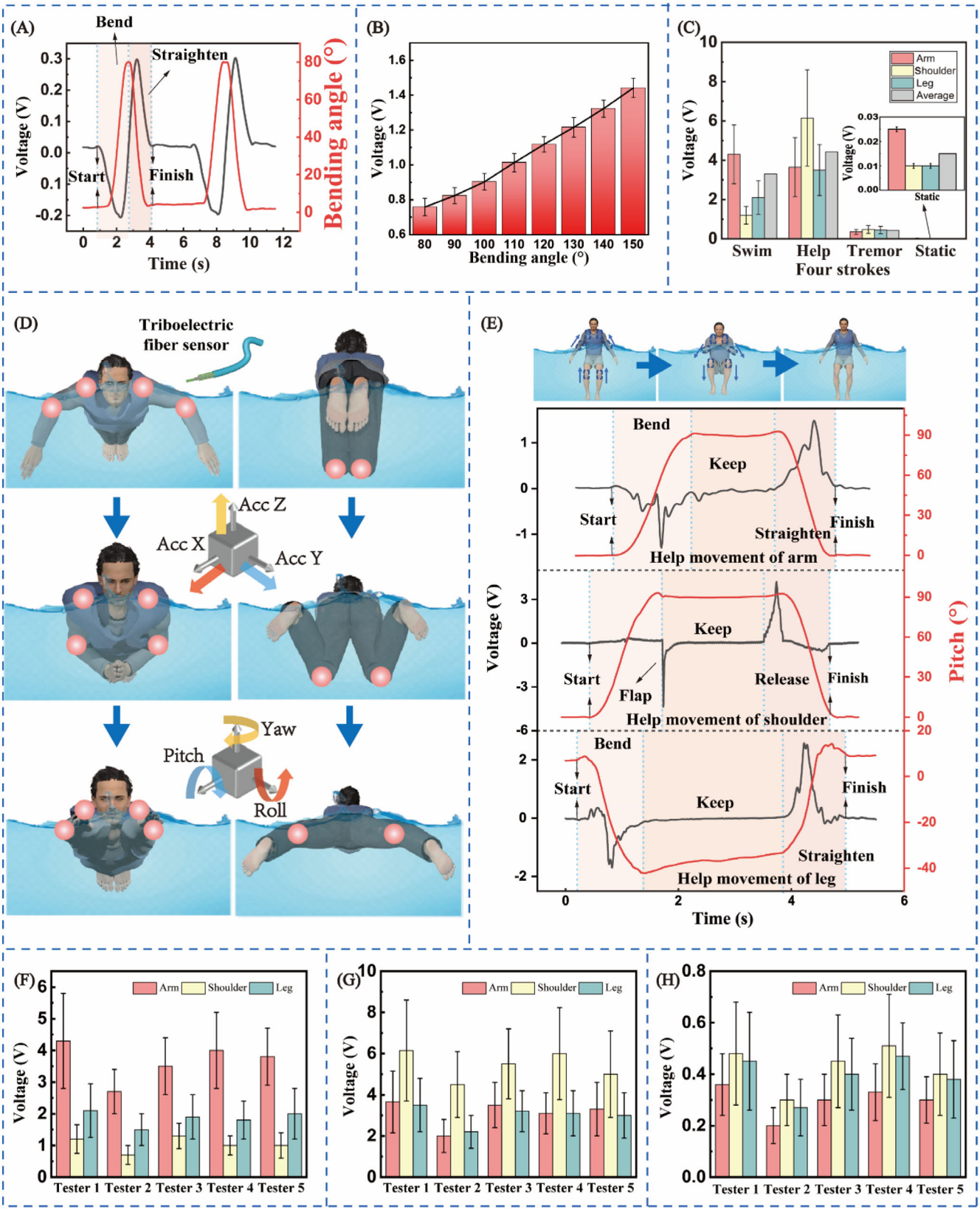

FIGURE 4 The signals comparison and analysis of joint bending and human movements utilizing SPLJ and commercial sensor. (A) The signal detail analysis of SPLJ during elbow bending process. (B) The output voltage of SPLJ at different elbow bending angles and their liner relationship. (C) Mean amplitude analysis of movement signals. (D) Schematic illustration of a swimmer model with monitoring components marked with solid red circles. (E) The signal detail analysis of SPLJ and commercial sensor during HELP position process. SPLJ's output performance with different height and weight subjects of (F) swimming state, (G) HELP posture state and (H) tremor state.

2.5 | Integrating deep learning analytics enables movements and condition recognition accuracy up to 100%

Machine learning, which has been proven to be an effective tool for automatically extracting features from the time-domain data of triboelectric signals and achieving high-precision recognition of different samples, has significantly advanced the field of signal analysis.[40] Figure 5A illustrates the workflow of machine learning analytics, depicting the process of posture recognition. Initially, the collected movement signals undergo preprocessing. After feature extraction and selection, a machine learning analytics is established between the feature matrix and labels, and then iterated subsequently. As the training data increases, the machine learning analytics gradually approaches the ground truth. Once the model is established, it can be used for human movement recognition. In signal processing, direct learning of time series data will incur huge costs in terms of both significant calculation time and memory space due to the large data volume. Therefore, feature extraction is a prerequisite for machine learning analytics.[41] In this study, multiple features of the data are learned, and the features that have the greatest impact on prediction accuracy are selected, including maximum value, minimum value, frequency, and peak-valley interval. Taking the extreme values as an example, the average amplitude of the movement signal peaks for each channel is extracted and illustrated in Figure 5B.

Deep learning analytics as a promising subfield of machine learning analytics has been applied for analyzing various sensory data due to wide adaptability and high accuracy. Specifically, convolutional neural networks (CNNs) in deep learning analytics have been widely demonstrated to be highly effective models for automatically extracting subtle features from time sequences of sensory outputs.[42–44] Thus, a CNN model is constructed as shown in Figure 5C. It is comprised by an input layer, hidden layers, and an output layer. To collect training data, the user is requested to perform four different movement states, including swimming state, HELP position state, tremor state, and static state.

The movement signals of the drowning person are captured by the portable circuit module, and the data is segmented into different data samples using a sliding window without overlap. For model training, these data samples with versatile information such as extreme values, frequency, movement time, maintenance time, and movement sequence are inputted to the model without requiring further data processing. The entire data set is divided into the training, testing, and validation sets using a 60%–20%–20% segmentation. The classification results for the drowning person's movements are presented in Figure 5D, demonstrating the accurate classification achieved by CNN with a 100% accuracy rate. The distribution of the data samples in the 2D feature space and the ROC curves are presented in Figure S19. This demonstrates the effectiveness of deep learning analytics in movement classification. Different classification methods yield varying performance. Clearly, the CNN (100%) classifier outperforms the logistic regression (97.5%) and linear discriminant (94.25%) classifiers, demonstrating higher classification accuracy (Figure S20). Due to its exceptional classification accuracy, versatility, robustness, and performance, the developed CNN model is established as an excellent choice for drowning person movement recognition sensors.

2.6 | Establishment of human condition detection system

To demonstrate the feasibility of SPLJ, a drowning person's condition detection system is developed, consisting of SPLJ, data acquisition and transmission modules, and a display module. When an individual falls into the water, the SPLJ accurately captures the drowning person's movement signals. The collected signals are then transmitted via WiFi to a computer for deep learning analytics, and upon completion, the results are exhibited on the computer interface. To demonstrate the applicability of the system in real-life situations, a pool is used to simulate water conditions. During the recognition process, the drowning person performs four different movements in the water, and these movement signals are received by the computer for deep learning analytics. The final prediction results are intuitively displayed on the computer monitor. The results are shown in Figure 5E–G, which demonstrate the movement process, while the upper-left section represents the underwater movement of the drowning person captured by an underwater camera. Information on the real-time waveform and total waveform is displayed on the left half of the software display interface, while the recognition results of the movement and condition of the individual are presented on the right half. The detailed monitoring process of the human condition detection system is described in Movies S1–S4. It can be observed that the developed system enables real-time monitoring of the drowning person's movement and condition. It provides vital information such as location and vital signs to rescue teams, serving as a theoretical basis for rescue plans and resource allocation, and ultimately improving the probability of successful ocean rescue operations.

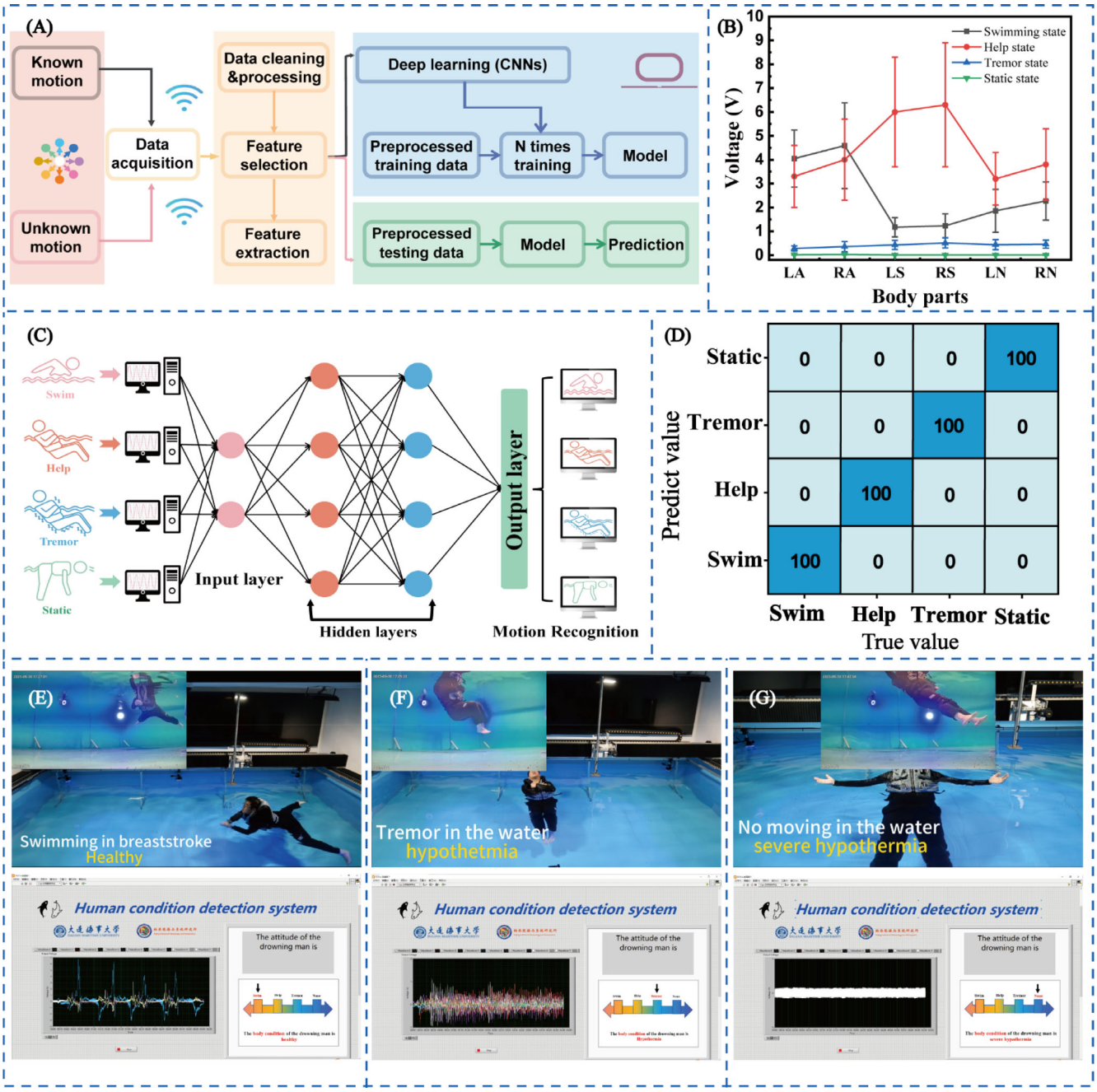

FIGURE 5 Deep learning analytics-based data processing for drowning person's movements and human condition detection system. (A) Flow diagram of deep learning analytics for drowning person's movements. (B) Average motion amplitude of different body parts and movements. (C) The developed CNN model for drowning person's movements. (D) Confusion map of the deep learning analytics for four movements. (E–G) The demonstration of human condition detection system for drowning people movements and condition.

3 | CONCLUSION

In this study, we have developed a closed-loop feedback system for drowning individual movements monitoring and distress rescue based on intelligent SPLJ, which is centered on WBAN technology and machine learning analysis. The SPLJ system converts human movement signals into electrical signals, which are then transmitted wirelessly to the rescue center. The rescue center analyzes signals to assess a person's condition in the water and formulate proper rescue strategies based on established correlations between movements and human condition. Multiple triboelectric fiber sensors are used as the basic sensing nodes of the SPLJ system due to their excellent ability to detect human joint movements. Furthermore, triboelectric fiber sensors possess exceptional

sensing capabilities, stretchability, and robustness making them highly potential in monitoring of environment and underwater flow. Through simulating various drown individual's movement under hypothermia, the correlation between the movement signals from SPLJ and the human condition is explored. Meanwhile, the effectiveness and universality of SPLJ in monitoring human movements will be verified through comparative experiments with multiple wearers using commercial monitoring sensors. Furthermore, a drowning people movement and condition monitoring system is developed using deep learning analytics, achieving a high accuracy recognition rate of 100%.

It is worth noting that SPLJ's capability in detecting mechanical movements under the underwater force field opens more opportunities that extend beyond intelligent survival devices. It has the potential to be applied in teaching activities like swimming, rescue operations, and diving. Additionally, it can additionally serve for monitoring human posture in various environments such as running, jumping, and other scenarios. In conclusion, this work presents a groundbreaking strategy for advanced underwater intelligent wearable survival devices, offering new opportunities for underwater rescue and ocean industry development.

4 | EXPERIMENTAL SECTION

4.1 | Materials

The silver wire was supplied by BOYIN. Ecoflex supersoft silicone (0030) was manufactured by Smooth-On, Inc. *N*,*N*-dimethylformamide (DMF) and P(VDF-TrFE) powder were supplied by Aladdin Reagent Co. Ltd. Swimsuit was purchased from Dongguan Power Clothing Co., LTD. Life jacket was purchased from Jiangsu Wuxi Qian Sports Life Saving Supplies Co., LTD. The cotton fabric was provided by Zhejiang Kaida Fabric Co., Ltd.

4.2 | Fabrication of triboelectric fiber sensor

4.2.1 | The triboelectric fiber sensor's core structure

The production equipment that could continuously produce core-sheath composite yarns on a large scale was manufactured by Tianjin Tianyuan Precision Machinery Co., Ltd. The winding silver wire is then cleaned by ultrasonication in ethanol and deionized water for 15 min. Next, 5.1 g of P(VDF-TrFE) is added to 24.9 g of *N*,*N*-dimethylformamide (DMF), and the mixture is stirred at 60°C for 2 h. After cooling, the mixture is uniformly coated on the silver wire, followed by air-drying at 80°C for 5 h, and this process is repeated five times. Finally, the coated fibers are annealed at 120°C under vacuum conditions for 2 h.

4.2.2 | The triboelectric fiber sensor's shell structure

The silver wire is wound tightly and uniformly on a polypropylene tube. Silicone rubber is then applied for five times to ensure uniform encapsulation of the silver wire. Next, the polypropylene tube is removed. The prepared inner core is inserted to create the necessary gap for contact-separation. Finally, the encapsulation process is completed using silicone rubber and the construction of triboelectric fiber sensor is finished.

4.3 | Fabrication of the SPLJ

The SPLJ is consisted of six triboelectric fiber sensors and a portable integrated circuit module (designed by Altium Designer 20 to draw the FPCB structure). The triboelectric fiber sensors are sewn to the shoulder and joints of the swimsuit by cloth and connected to the portable integrated circuit module by varnished wires to collect and transmit movement signals from the body.

4.4 | Characterization and measurement

The surface of P(VDF-TrFE) fiber and triboelectric fiber sensor is characterized by AW31 optical microscope and Nova Nanosem 450 field emission scanning electron microscope. A linear motor (LinMot E1100) is used to impact triboelectric fiber sensor. A system based on a programmable electrometer (Keithley, Model 6514) and a software which built by LabVIEW platform is used to test the output performance including VOC, ISC, and QSC. The COSMOL software is used to simulate the spatial potential distribution. The deep learning analytics is used to preprocess and classify the gait data by MATLAB programming. The human condition detection system and interaction interface are achieved by calling the pretrained program in MATLAB through the LabVIEW.

ACKNOWLEDGMENTS

The authors are grateful for the support received from the Natural Science Foundation of the Beijing Municipality (grant nos. L222037, 2212052), the National Natural

Science Foundation of China (grant no. 22109012), and the Fundamental Research Funds for the Central Universities (grant no. E1E46805). No formal approval for the experiments involving human volunteers was required. The volunteers took part following informed consent.

CONFLICT OF INTEREST STATEMENT

The authors declare no conflict of interest.

ORCID

Chuanhui Wei https://orcid.org/0000-0001-8054-3424
Kai Dong https://orcid.org/0000-0001-6314-1546

REFERENCES

1. Pointer K, Milligan GS, Garratt KL, Clark SP, Tipton MJ. A 10-year descriptive analysis of UK maritime and coastguard data on lifejacket use and drowning prevention. *Safety Sci*. 2018;109:195-200.
2. Hansen HL, Jepsen JR, Hermansen K. Factors influencing survival in case of shipwreck and other maritime disasters in the Danish merchant fleet since 1970. *Safety Sci*. 2012;50(7):1589-1593.
3. Quistberg DA, Bennett E, Quan L, Ebel BE. Low life jacket use among adult recreational boaters: a qualitative study of risk perception and behavior factors. *Accid Anal Prev*. 2014;62:276-284.
4. Pitman SJ, Wright M, Hocken R. An analysis of lifejacket wear, environmental factors, and casualty activity on marine accident fatality rates. *Safety Sci*. 2019;111:234-242.
5. Jiang Y, Jiang J, Zhang C, Zhang W, Gao Y, Mi C. A copula-based battery pack consistency modeling method and its application on the energy utilization efficiency estimation. *Energy*. 2019;189:116219.
6. Han Z, Wang W, Du Z, Zhang Y, Yu Y. Self-heating inflatable lifejacket using gas generating agent as energy source. *Energy*. 2021;224:120087.
7. Zou Y, Tan P, Shi B, et al. A bionic stretchable nanogenerator for underwater sensing and energy harvesting. *Nat Commun*. 2019;10(1):2695.
8. Li C, Liu D, Xu C, et al. Sensing of joint and spinal bending or stretching via a retractable and wearable badge reel. *Nat Commun*. 2021;12(1):2950.
9. Gunawardhana KRSD, Wanasekara ND, Dharmasena RDIG. Towards truly wearable systems: optimizing and scaling up wearable triboelectric nanogenerators. *iScience*. 2020;23(8):101360.
10. Meng X, Cheng Q, Jiang X, et al. Triboelectric nanogenerator as a highly sensitive self-powered sensor for driver behavior monitoring. *Nano Energy*. 2018;51:721-727.
11. Wang C, Hu K, Li W, et al. Wearable wire-shaped symmetric supercapacitors based on activated carbon-coated graphite fibers. *ACS Appl Mater Interfaces*. 2018;10(40):34302-34310.
12. Wang C, Liu Y, Qu X, et al. Ultra-stretchable and fast self-healing ionic hydrogel in cryogenic environments for artificial nerve fiber. *Adv Mater*. 2022;34(16):2105416.
13. Salauddin M, Rana SMS, Rahman MT, et al. Fabric-assisted MXene/silicone nanocomposite-based triboelectric nanogenerators for self-powered sensors and wearable electronics. *Adv Funct Mater*. 2022;32(5):2107143.
14. Dassanayaka DG, Alves TM, Wanasekara ND, Dharmasena IG, Ventura J. Recent progresses in wearable triboelectric nanogenerators. *Adv Funct Mater*. 2022;32(44):2205438.
15. Shen H, Lei H, Gu M, et al. A wearable electrowetting on dielectrics sensor for real-time human sweat monitor by triboelectric field regulation. *Adv Funct Mater*. 2022;32(34):2204525.
16. Abiodun AS, Anisi MH, Khan MK. Cloud-based wireless body area networks: managing data for better health care. *IEEE Consum Electron Mag*. 2019;8(3):55-59.
17. Xu P, Zheng J, Liu J, et al. Deep-learning-assisted underwater 3D tactile tensegrity. *Research*. 2023;6:0062.
18. Xu P, Liu J, Liu X, et al. A bio-inspired and self-powered triboelectric tactile sensor for underwater vehicle perception. *npj Flex Electron*. 2022;6(1):25.
19. Xu P, Wang X, Wang S, et al. A triboelectric-based artificial whisker for reactive obstacle avoidance and local mapping. *Research*. 2021;2021:9864967.
20. Liu J, Xu P, Zheng J, et al. Whisker-inspired and self-powered triboelectric sensor for underwater obstacle detection and collision avoidance. *Nano Energy*. 2022;101:107633.
21. Gu GQ, Han CB, Tian JJ, et al. Triboelectric nanogenerator enhanced multilayered antibacterial nanofiber air filters for efficient removal of ultrafine particulate matter. *Nano Res*. 2018;11(8):4090-4101.
22. Jiang F, Shan Y, Tian J, et al. Poly(L-lactic acid) nanofiber-based multilayer film for the electrical stimulation of nerve cells. *Adv Mater Interfaces*. 2023;10(17):2202474.
23. Fan FR, Tian ZQ, Wang ZL. Flexible triboelectric generator! *Nano Energy*. 2012;1(2):328-334.
24. Wang ZL. Triboelectric nanogenerators as new energy technology for self-powered systems and as active mechanical and chemical sensors. *ACS Nano*. 2013;7(11):9533-9557.
25. Zi YL. Effective energy storage from a triboelectric nanogenerator. *Nat Commun*. 2016;7(1):10987.
26. Chun JS. Boosted output performance of triboelectric nanogenerator via electric double layer effect. *Nat Commun*. 2016;7(1):12985.
27. Xu W, Liu S, Yang J, et al. Self-powered flexible handwriting input panel with 1D output enabled by convolutional neural network. *Nano Energy*. 2022;101:107557.
28. Li Y, Xiao K, Huang C, et al. Enhanced potassium-ion storage of the 3D carbon superstructure by manipulating the nitrogen-doped species and morphology. *Nano-Micro Lett*. 2021;13(1):1.
29. Han Y, Yi F, Jiang C, et al. Self-powered gait pattern-based identity recognition by a soft and stretchable triboelectric band. *Nano Energy*. 2019;56:516-523.
30. Zeng Y, Xiang H, Zheng N, Cao X, Wang N, Wang ZL. Flexible triboelectric nanogenerator for human motion tracking and gesture recognition. *Nano Energy*. 2022;91:106601.
31. Durukan MB, Cicek MO, Doganay D, Gorur MC, Çınar S, Unalan HE. Multifunctional and physically transient supercapacitors, triboelectric nanogenerators, and capacitive sensors. *Adv Funct Mater*. 2022;32(1):2106066.
32. Cai F, Yi C, Liu S, et al. Ultrasensitive, passive and wearable sensors for monitoring human muscle motion and physiological signals. *Biosens Bioelectron*. 2016;77:907-913.
33. Guo H, Pu X, Chen J, et al. A highly sensitive, self-powered triboelectric auditory sensor for social robotics and hearing aids. *Sci Robot*. 2018;3(20):eaat2516.

34. Zhao H, Xiao X, Xu P, et al. Dual-tube Helmholtz resonator-based triboelectric nanogenerator for highly efficient harvesting of acoustic energy. *Adv Energy Mater*. 2019;9(46):1902824.
35. Yu H, Xi Z, Zhang Y, et al. High performance additional mass enhanced film structure triboelectric nanogenerator for scavenging vibration energy in broadband frequency range. *Nano Energy*. 2023;107:108182.
36. Zhang Y, Li Y, Cheng R, et al. Underwater monitoring networks based on cable-structured triboelectric nanogenerators. *Research*. 2022;2022(2):12.
37. Wang J, Wu C, Dai Y, et al. Achieving ultrahigh triboelectric charge density for efficient energy harvesting. *Nat Commun*. 2017;8(1):88.
38. Lai M, Du B, Guo H, et al. Enhancing the output charge density of TENG via building longitudinal paths of electrostatic charges in the contacting layers. *ACS Appl Mater Interfaces*. 2018;10(2):2158-2165.
39. Elble RJ. Tremor amplitude is logarithmically related to 4- and 5-point tremor rating scales. *Brain*. 2006;129(10):2660-2666.
40. Zhou Z, Chen K, Li X, et al. Sign-to-speech translation using machine-learning-assisted stretchable sensor arrays. *Nat Electron*. 2020;3(9):571-578.
41. Englehart K, Hudgins B. A robust, real-time control scheme for multifunction myoelectric control. *IEEE Trans Biomed Eng*. 2003;50(7):848-854.
42. Shi Q, Zhang Z, He T, et al. Deep learning enabled smart mats as a scalable floor monitoring system. *Nat Commun*. 2020;11(1):4609.
43. Wen F, Sun Z, He T, et al. Machine learning glove using self-powered conductive superhydrophobic triboelectric textile for gesture recognition in VR/AR applications. *Adv Sci*. 2020;7(14):2000261.
44. Jin T, Sun Z, Li L, et al. Triboelectric nanogenerator sensors for soft robotics aiming at digital twin applications. *Nat Commun*. 2020;11(1):5381.

SUPPORTING INFORMATION

Additional supporting information can be found online in the Supporting Information section at the end of this article.

How to cite this article: Zhang Y, Li C, Wei C, et al. An intelligent self-powered life jacket system integrating multiple triboelectric fiber sensors for drowning rescue. *InfoMat*. 2024;e12534. doi:10.1002/inf2.12534